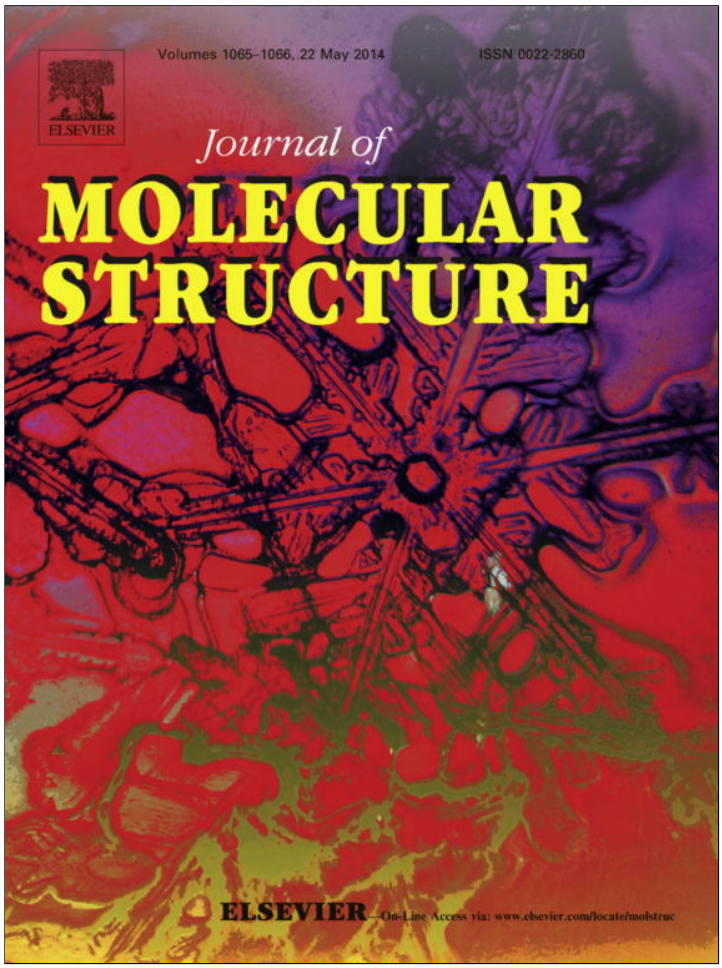

Journal of Molecular Structure 1065-1066 (2014) 160–169

Contents lists available at ScienceDirect

Journal of Molecular Structure

journal homepage: www.elsevier.com/locate/molstruc

An experimental study of the structural and vibrational properties of sesquiterpene lactone cnicin using FT-IR, FT-Raman, UV–visible and NMR spectroscopies

Fernando Chain [a], Elida Romano [b], Patricio Leyton [c], Carolina Paipa [d], César Atilio Nazareno Catalán [a], Mario Antonio Fortuna [e], Silvia Antonia Brandán [b,*]

[a] INQUINOA-CONICET, Instituto de Química Orgánica, Facultad de Bioquímica Química y Farmacia, Universidad Nacional de Tucumán, Ayacucho 471, 4000 S.M. de Tucumán, Tucumán, Argentina
[b] Cátedra de Química General, Instituto de Química Inorgánica, Facultad de Bioquímica, Química y Farmacia, Universidad Nacional de Tucumán, Ayacucho 471, 4000 San Miguel de Tucumán, Tucumán, Argentina
[c] Instituto de Química, Pontificia Universidad Católica de Valparaíso, Valparaíso, Chile
[d] Departamento de Ciencias Químicas, Facultad de Ciencias Exactas, Universidad Andrés Bello (UNAB), Quillota 910, Viña del Mar, Chile
[e] Cátedra de Química Orgánica, Dpto. Cs. Básicas, Facultad de Agronomía y Zootecnia, Universidad Nacional de Tucumán, Av. Néstor Kirchner, 4000 San Miguel de Tucumán, Tucumán, Argentina

HIGHLIGHTS

- Cnicin was characterized by infrared, Raman, NMR and UV–visible spectroscopies.
- The molecular structure of cnicin has a ten member's ring with a chair conformation.
- The γ-lactone ring of cnicin has a half-chair conformation.
- The NBO and AIM studies show the high stability of cnicin.
- A complete assignment of the 153 normal vibration modes for cnicin was performed.

GRAPHICAL ABSTRACT

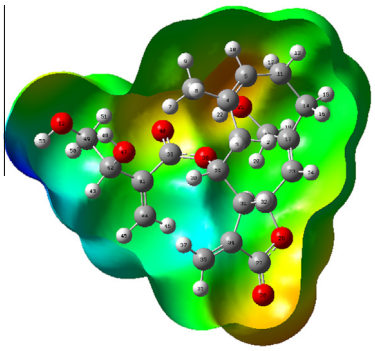

ARTICLE INFO

Article history:
Received 7 October 2013
Received in revised form 19 February 2014
Accepted 19 February 2014
Available online 12 March 2014

Keywords:
Cnicin
Vibrational spectra
Molecular structure
Force field
DFT calculations

ABSTRACT

An experimental and theoretical investigation of cnicin is presented, combining the use of infrared, Raman, NMR and UV–visible spectroscopies with density functional theory (DFT) that employs hybrid B3LYP exchange correlation functional and a 6-31G* basis set. The molecular electrostatic potentials, atomic charges, bond orders, stabilization energies, topological properties and energy gap are presented by performing NBO, AIM and HOMO–LUMO calculations at the same level of theory as cnicin. A complete vibrational compound assignment was performed by employing internal coordinate analysis and a scaled quantum mechanical force field (SQMFF) methodology. Comparisons between the theoretical and experimental vibrational and ultraviolet–visible spectra show a strong concordance. The geometrical parameters and NBO studies suggest a probable negative Cotton effect for cnicin, which can be attributed to the $\pi \rightarrow \pi^*$ transition for an α,β-unsaturated γ-lactone, as reported in the literature.

* Corresponding author. Tel.: +54 381 4247752; fax: +54 381 4248169.
E-mail address: sbrandan@fbqf.unt.edu.ar (S.A. Brandán).

http://dx.doi.org/10.1016/j.molstruc.2014.02.057
0022-2860/

1. Introduction

As part of our investigation of compounds of great pharmacological importance that contain structural rings [1–23], we have considered the sesquiterpene lactone (SL) cnicin, whose IUPAC chemical name is [(3aR,4S,6E,10Z,11aR)-10-(hydroxymethyl)-6-methyl-3-methylidene-2-oxo-3a,4,5,8,9,11a-hexahydrocyclodeca[b]furan-4-yl](3R)-3,4-dihydroxy-2-methylidenebutanoate. This SL has been extensively investigated for its multiple biological activities, including its anti-diabetic, anti-diarrheic, anti-rheumatic, anti-inflammatory, anti-pyretic and antibacterial effects [24–31]. Recent advances in therapy show that the cytotoxic activity of cnicin in multiple myeloma possesses potent anti-proliferative effects and induces death of primary myeloma cells even in the presence of survival cytokines in the tumor microenvironment [32]. Therefore, cnicin arises as a new anti-tumor drug and underlines the potential usefulness of sesquiterpene lactones in tumor therapy [32]. Most current studies are oriented towards the development of chemotherapeutic agents with less adverse reactions, such as the one that tries to find new pyridine based antitumoral drugs with the use of structure–activity relationship (SAR) methods [33]. Therefore, understanding the structural and vibrational properties of cnicin is vital for drug design, as all of the potential structural modifications of cnicin should be related to the improvement of its biological activities. Many investigations have been performed from this point of view [24–32]; however, there is minimal information on the structural and vibrational properties of cnicin, as its molecular structure has not been determined and its vibrational spectrum has not been assigned. Hence, the aims of this work are to study its structural properties, such as the molecular electrostatic potentials, atomic charges, bond orders, stabilization energies, topological properties and energy gap using the NBO [34,35], AIM [36,37] and HOMO–LUMO [38] calculations for which the theoretical structure was optimized and the corresponding harmonic frequencies were calculated. In addition, the complete assignment of the bands observed in the vibrational spectrum was completed by combining the experimental infrared and Raman spectra with DFT calculations, internal symmetry coordinates and a generalized valence force field (GVFF) [39]. In addition, the force constants were also reported, and the comparisons between the corresponding experimental NMR and UV–visible spectra are in strong agreement with the theoretical ones. All calculated properties are analyzed and discussed.

2. Experimental methods

Cnicin was isolated from *Centaurea* (Asteraceae), as reported in previous papers [29–31], and the compound was characterized by infrared, Raman, NMR and UV–visible spectroscopies. The UV, EI–MS, ^{1}H and ^{13}C NMR spectra were identical to those previously reported [29–31]. Purity was determined to be >99.98% using capillary gas chromatography with both a flame ionization detector (FID) and selective mass detector.

The FT-IR spectrum in the region of 4000–400 cm^{-1} was recorded on a Fourier Transform Infrared (FT-IR) Perkin–Elmer Spectrum RX spectrometer equipped with a DTGS (Deuterated TriGlycerine Sulfate) detector. The spectral resolution was 2 cm^{-1}, and 16 scans were performed. The spectrum was measured by placing one drop of the pure sample between the KBr windows. The Raman spectrum was recorded with a RM2000 Renishaw Raman Microscope System equipped with a diode laser, providing a 634 nm line, a Leica microscope, an electrically cooled CCD (Charge Coupled Device) detector and a notch filter to eliminate elastic scattering. The spectrum was obtained using a 50× objective. The laser power output was 2.0 mW, and the spectral resolution was 2 cm^{-1}.

Nuclear Magnetic Resonance (NMR) spectra were acquired using a Bruker Avance III instrument at 200 MHz (^{1}H) and 50 MHz (^{13}C) with DMSO-d_6 as a solvent. GC–MS analysis was performed using a Hewlett-Packard 6890 system with a Hewlett-Packard 5973 mass selective detector and a Perkin–Elmer Elite-5MS column (5% phenylmethyl siloxane, 30 m length × 0.25 mm inner diameter × 0.25 μm film thickness) with He as carrier gas (1 mL/min; constant flow). The injector, GC–MS interphase, ion source and selective mass detector temperatures were maintained at 280, 280, 230 and 150 °C, respectively. The UV spectra were recorded on a Shimadzu 160A UV–visible spectrophotometer.

3. Computational details

The initial structure of cnicin was modeled with the *GaussView* program [40] and was later optimized at the B3LYP/6-31G* level of theory [41,42] using the Gaussian 09 package program [43]. For this structure, the potential energy surface curves were studied modifying the C29—O38—C39—O40, O38—C39—C41—C42, C41—C42—C49—O52, C39—C41—C42—C49 and C42—C49—O52—H53 dihedral angles. Thus, eight conformations with similar energies and population analysis were found. Table S1 shows a comparison of the total energies for those stable structures of cnicin together with the corresponding dipole moment values by using the B3LYP/6-31G* method. The population analysis show similar values among the different structures, for this reason, in this study, we have considered the C1 structure in accordance with the stable structure of another sesquiterpene lactone onopordopicrin (*Vibrational and structural study of onopordopicrin based on FTIR and FT-Raman spectra and DFT calculations by Chain et al.*) whose structure has a side chain similar to cnicin, as can be seen in Fig. S1 (Supporting Material). The considered stable structure with C_1 symmetry can be seen in Fig. 1 together with the labeled atoms. A detailed structure showing the two rings of five members (A5) and of ten members (A10) is given in Fig. S1. The optimized cnicin structure was analyzed using the natural population atomic (NPA) and the charges derived from Merz–Kollman [44], while the bond orders were also calculated at the same theory levels from the NBO calculation using the NBO 3.1 program [35], as implemented in the Gaussian 09 package [43]. The AIM2000 program [37] was used to perform the topological analysis, while the harmonic force field for cnicin was evaluated at the B3LYP/6-31G* level using the SQMFF procedure [39] with the Molvib program [45]. This later program was also employed to transform the resulting force fields to "natural" internal coordinates. The natural internal coordinates for cnicin are listed in Table S2, and they were defined as those reported for compounds with similar groups [1,2,4–7,9–11,17–23]. The complete assignment was then performed, taking into account the resulting SQM and the potential energy distribution components (PED) $\geqslant$10%. The nature of all of the vibration normal modes was ascertained by means of the *GaussView* program [40]. For cnicin, the calculated chemical shifts of the ^{1}H NMR and ^{13}C NMR spectra were obtained from the GIAO method [46] using the B3LYP/6-311++G** level of theory, as better results are obtained from using this theory level. Therefore, the calculations were performed using the geometries optimized for this level of theory, using TMS as reference. The ultraviolet–visible spectrum was predicted using TD-DFT calculations at the B3LYP/6-31G* theory level with the Gaussian 09 program [43].

4. Results and discussion

4.1. Geometry optimization

Table 1 shows a comparison of the calculated geometrical parameters for cnicin using the B3LYP/6-31G* method, with the experimental values determined for costunolide by means of

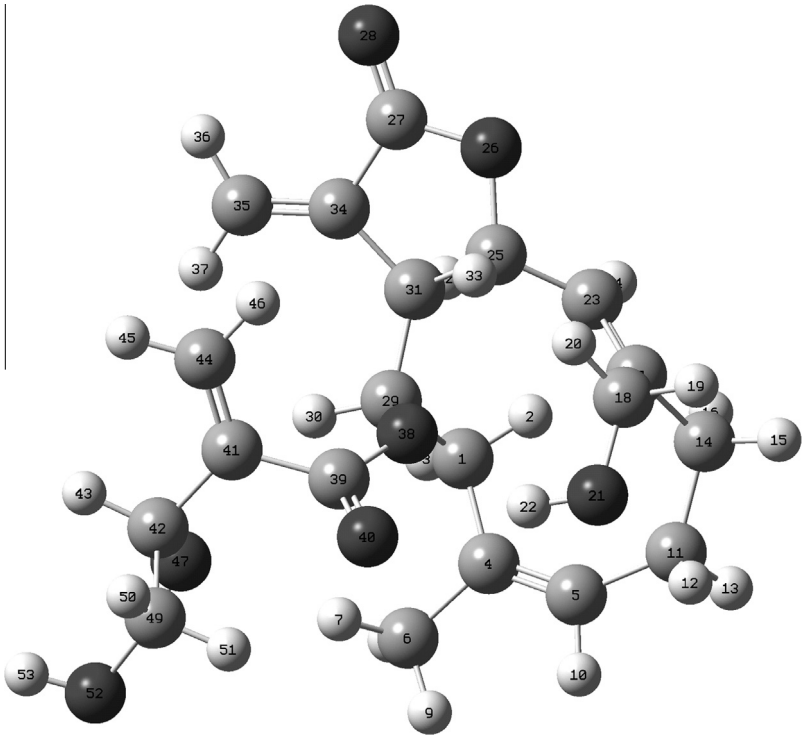

Fig. 1. Molecular structure of cnicin and atoms numbering.

X-ray diffraction, as demonstrated by Bovill et al. [47]. The sesquiterpenic germacranolide costunolide has two fused rings, one planar with five members and the other with ten members that adopt a chair conformation (Fig. S1). The bond length and bond angle comparisons were expressed in terms of root-mean-square deviation (RMSD) values and reveal that the bond lengths have a better correlation (0.004 Å) than the bond angles (1.3°) using the B3LYP/6-31G* calculation level. In this compound, as in the sesquiterpenoid 9,10-dihydrofukinone [23], greater differences between both compared compounds are observed in the dihedral angles (18.7°). In cnicin, the difference between the C4—C5—C11—C14 and C35—C34—C27—O28 dihedral angle values justify such variations. The double bonds belonging to the ten-membered ring, C4=C5 and C17=C23, are predicted to be longer than the experimental values of 1.326 and 1.329 Å, respectively. On the other hand, the corresponding involved C—C=C—C dihedral angles, C1—C4=C5—C11 (2.5°) and C14—C17=C23—C25 (152.2°), are predicted to be smaller than the experimental values, as observed in Table 1 [47]. In addition, the calculations for cnicin in the gas phase are also applicable to the solid phase, as demonstrated by Bovill et al. [47]. The mean bond lengths for the Csp^3–Csp^3, Csp^3–Csp^2, and C=C distances are approximately 1.545, 1.500, and 1.323 Å, respectively. On the other hand, the calculations predicted a value of −7.7° for the exocyclic C=C—C=O dihedral angle torsion of the lactone in cnicin, while the experimental value for the sesquiterpenoid costunolide is −10°. In cnicin, as in costunolide, the γ-lactone ring has a half-chair conformation between the C25 and C31 atoms, which is characteristic of a *trans* lactone with negative C=C—C=O torsion angles.

To evaluate the distribution of charges on all of the atoms of cnicin and its structural stability, the potential energy and the dipole moment values were calculated using the B3LYP/6-31G* method. The results demonstrate that the molecule has a certain polarity with a dipole moment value of 5.74*D* as expected, as cnicin has —OH and —COO groups in its structure with a corresponding potential energy of −1304.2208 Hartrees. To analyze the structural properties of cnicin, the molecular electrostatic potential and the types of three different charges were calculated. The Mulliken, natural atomic charges (NPA) and those derived from the Merz-Kollman (MK) charges were calculated using a 6-31G* basis set; their values are given in Table S3 together with the molecular electrostatic potential values. The three charges here are considered to have different values, with the Mulliken charges being approximately the same as the MK charges. The results demonstrate that the negative high atomic charge values are located on the five O atoms of cnicin, while the positive high atomic charge values are observed on the H atoms belonging to the —OH and —C=CH_2 groups. The stability of cnicin is thus associated with the charge distribution and the presence of both O atoms and C=C bonds that give cnicin a particular polarity. In analyzing the molecular electrostatic potential, we observed that the higher values are located on the five O atoms of cnicin and the C atoms belonging to the ten-member ring. A strong red color on the O atoms and a blue color on the H atoms are then expected on the surface of cnicin, as observed in Fig. S2. The red color observed here is related to the potential nucleophilic sites while the blue color is associated with potential electrophilic regions.

4.2. NBO study

The stability of cnicin was also studied with NBO calculations [35] using a 6-31G* basis set in terms of bond orders, expressed as Wiberg indexes and second order perturbation energies, which are given in Table S3. The bond order values clearly show higher values for the C4, C5, C17, C23, C27, C34, C35, C39, C41, atoms (between 4.004 and 3.820), as expected because they are involved in double bonds. For this reason, they have sp^2 hybridization, while the lower bond order values are observed in the C atoms with sp^3 hybridization. On the other hand, the bond orders corresponding to the O26 and O38 atoms have the highest values (2.151 and 2.145, respectively) than the other ones (O28, O40, O47, O52).

Table S4 shows the second-order perturbation energies $E^{(2)}$ (donor → acceptor) related to the most important delocalizations observed for gaseous cnicin at a B3LYP/6-31G* level of theory.

Table 1
Calculated geometrical parameters for cnicin.

Parameter	6-31G*[a]	Exp.[b]
Bond length (Å)		
C1—C4	1.513	1.500 (3)
C4—C5	1.345	1.326 (3)
C4—C6	1.515	1.496 (3)
C5—C11	1.521	1.485 (3)
C11—C14	1.554	1.555 (3)
C14—C17	1.513	1.512 (3)
C17—C23	1.346	1.329 (2)
C23—C25	1.488	1.483 (2)
C25—C31	1.557	1.544 (2)
C25—O26	1.456	1.473 (2)
O26—C27	1.368	1.348 (2)
C27—C34	1.504	1.483 (3)
C27—O28	1.205	1.204 (3)
C34—C35	1.332	1.315 (3)
C31—C34	1.506	1.506 (2)
C31—C29	1.544	1.536 (2)
C1—C29	1.568	1.546 (3)
C17—C18	1.522	1.487 (3)
C18—O21	1.416	
C29—O38	1.455	
C39—O38	1.351	
C39—O40	1.214	
C39—C41	1.505	
C41—C44	1.336	
C41—C42	1.509	
C42—O47	1.424	
C42—C49	1.539	
C49—O52	1.430	
RMSD	0.004	
Bond angle (degrees)		
C1—C4—C5	126.1	127.1 (1)
C1—C4—C6	114.4	114.5 (2)
C5—C4—C6	119.2	123.8 (2)
C4—C5—C11	139.0	127.7 (2)
C5—C11—C14	126.3	109.8 (2)
C11—C14—C17	115.9	108.8 (2)
C14—C17—C23	118.5	117.9 (2)
C17—C23—C25	125.3	126.1 (2)
C23—C25—O26	115.5	110.8 (1)
C25—O26—C27	109.4	110.4 (1)
O26—C27—O28	122.9	121.7 (2)
O26—C27—C34	108.8	109.1 (1)
O28—C27—C34	128.2	129.2 (2)
C27—C34—C35	122.0	120.8 (2)
C31—C34—C35	132.3	131.5 (2)
C29—C31—C34	124.0	114.8 (1)
C27—C34—C31	105.4	107.7 (1)
C1—C29—C31	108.9	117.4 (1)
C4—C1—C29	117.7	114.9 (2)
RMSD	1.3	
Dihedral angles (degrees)		
C27—O26—C25—C23	149.5	145.1 (1)
C25—O26—C27—O28	168.3	172.7 (2)
C4—C5—C11—C14	5.0	−101.8 (2)
C11—C5—C4—C6	179.1	−13.6 (3)
C11—C14—C17—C23	−121.1	−88.6 (2)
C14—C17—C23—C25	152.2	155.6 (2)
C17—C23—C25—O26	139.4	110.5 (2)
O26—C25—C31—C29	−168.8	−149.9 (1)
C23—C25—C31—C29	67.4	88.6 (2)
C25—C31—C29—C1	−87.9	−83.9 (2)
C25—C31—C34—C27	26.9	20.5 (2)
C29—C31—C34—C27	155.0	146.4 (1)
C31—C29—C1—C4	151.3	73.6 (2)
C29—C1—C4—C6	75.5	66.7 (2)
C31—C34—C27—O28	168.4	170.0 (2)
C35—C34—C27—O28	−7.7	171.8 (2)
RMSD	18.7	

[a] This work.
[b] From Ref. [47].

The results demonstrate three types of contributions to the stabilization energies, which are mainly due to the presence of double bonds and the free electron pairs of the oxygen atoms, which are the $\Delta ET_{\sigma\to\sigma*}$, $\Delta ET_{LP\to\sigma*}$ and $\Delta ET_{\sigma*\to\sigma*}$ charge transfers. The total energy contribution is principally due to the lone pairs of the oxygen atoms ($\Delta ET_{LP\to\sigma*}$), which clearly show that the highest stability of cnicin is related to the presence of the —OH groups, the —COO group and the lactone ring.

4.3. AIM analysis

The electrostatic interactions of cnicin were also studied, employing Bader's atoms in molecules theory [36] by using the AIM2000 program [37]. The topological property calculations, such as electron charge density (ρ) and *Laplacian* values $\nabla^2\rho(r)$ in the bond critical points (BCPs) are shown in Table S5. The critical points have three principal characteristics: the $\rho(r)$ values should be between 0.05 and 0.3 a.u., the relationship $|\lambda_1|/\lambda_3$ should be <1 and the Laplacian of the electron density $\nabla^2\rho(r)$ should be positive and have values between 0.04 and 0.2 a.u., indicating that the interaction is dominated by the contraction of charge away from the interatomic surface toward each nucleus [2–14,17,19–23]. This analysis clearly shows ten BCPs, of which seven are O—H hydrogen bonds, one is a C—C bond, one is a C—H bond and one is an H—H bond, as observed in Table S5. In the OH—H BCPs, the $\rho(r)$ values are slightly dependent on the involved distance; therefore, a higher density (0.0227 a.u.) is observed for the O52—H48 bond because there is a lower distance between both atoms (2.095 Å). On the contrary, the density in the C—H bond is 0.0152 a.u. (for a 2.386 Å distance), which is slightly higher than expected for the O38—H22 BCP, although the distance between these atoms is 2.354 Å. For the remaining H20—H33 BCP, the density value is 0.0121 a.u. with a distance between atoms of 2.010 Å. In general, the results clearly reveal that the topological properties of the BCPs are more dependent on the nature of the interactions than the distances between the involved atoms. Moreover, this analysis shows that the high stability of cnicin is related to the presence of three different hydrogen bonds, as shown in Table S5.

4.4. NMR analysis

A comparison of the ^{1}H and ^{13}C NMR spectroscopic data for cnicin in DMSO-d6 with the theoretical values calculated for the compound using the GIAO method [46] and the 6-31G* and 6-311++G** basis sets can be seen in Tables S6 and S7, respectively. The ^{1}H NMR spectrum for cnicin in DMSO-d6 is given in Fig. S3, while Fig. S4 shows the corresponding ^{13}C NMR spectrum. The calculated shifts for the ^{1}H nucleus by using both basis sets and the experimental values were compared with those reported for cnicin by Berger and Sicker [48] by means of the RMSD values. In general, the RMSD values strongly agree with both basis sets (0.62 and 0.69 ppm, respectively, by using 6-31G* and 6-311++G** basis sets). The calculated shifts for the H2 and H15 nuclei are higher than the experimental values; therefore, they show higher differences because their peaks overlap with the bands corresponding to DMSO-d_6. Additionally, the formation of the O38—H22 and O52—H48 bonds justify that the experimental shifts for the H22 and H48 nuclei are not observed, as seen in Table S5. On the other hand, the calculated shifts for the ^{13}C nucleus using both basis sets with our experimental values were compared with those reported for cnicin by Berger and Sicker [48] using RMSD values (10.2 and 9.00 ppm, respectively, by using 6-31G* and 6-311++G** basis sets). In this case, the calculated ^{13}C chemical shifts for cnicin

demonstrate a stronger concordance by using the 6-311++G** basis set, as expected based on the experimental data reported for other compounds containing similar groups [13,16,18,23]. Another important finding is that the theoretical calculations do not correctly predict the chemical shifts for the C23 and C35 nuclei, most likely because these atoms are involved in the C35—C44 and C23—H2 intermolecular H-bonds, as demonstrated by the AIM calculations (Table S5).

4.5. Vibrational analysis

Figs. 2 and 3 show comparisons between the recorded infrared and Raman spectra, respectively, for cnicin with the corresponding theoretical spectra calculated using the 6-31G* basis set. The optimized cnicin structure has C_1 symmetry and 153 normal vibration modes, which are all active in both the infrared and Raman spectra. The assignment of the experimental bands to the normal modes of vibration was performed at the B3LYP/6-31G* level of theory using SQMFF methodology [39] and taking into account the Potential Energy Distribution (PED) calculated with the Molvib program [45]. Table 2 shows the corresponding experimental and SQM-calculated wavenumbers based on the B3LYP/6-31G* calculations together with the assignments for the expected normal vibration modes of cnicin. This calculation level was used because the scale factors are only defined for the 6-31G* basis set [39]. As observed in Table S8, some vibration modes corresponding to the CH_2 groups appear strongly mixed and have minimal PED contribution, while other modes, such as the CCO or CCC deformations, do not appear due to their coupling with different vibration modes. In both cases, the assignments of those modes were completed with the aid of the *GaussView* program [40]. A characteristic symbol identifies those modes, as indicated in Table 2. Below, we discuss the assignment of selected groups.

4.5.1. Band assignments

4.5.1.1. OH modes. The shoulders and IR band observed between 3404 and 3246 cm^{-1} are assigned to the three expected OH stretchings. In accordance with the compounds containing OH

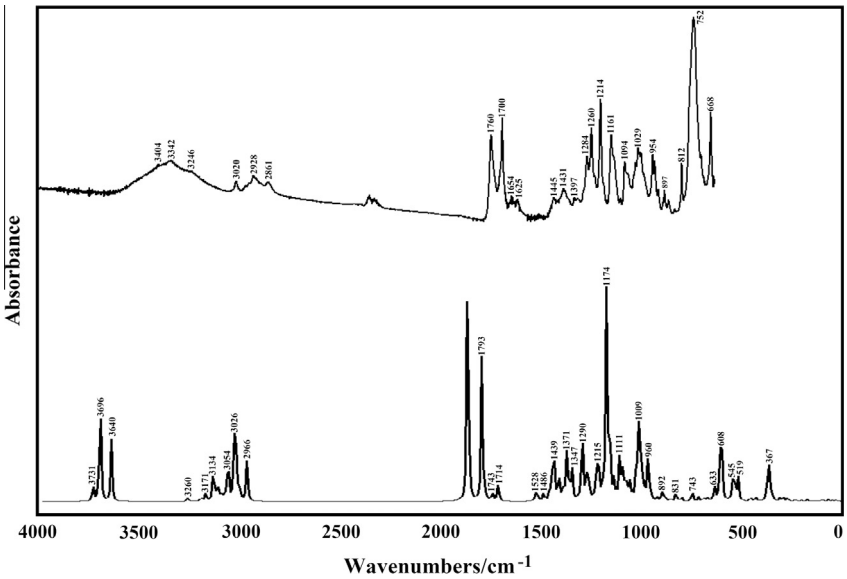

Fig. 2. Comparison between the experimental infrared spectrum of cnicin (upper) with the corresponding theoretical at B3LYP/6-31G* level of theory (bottom).

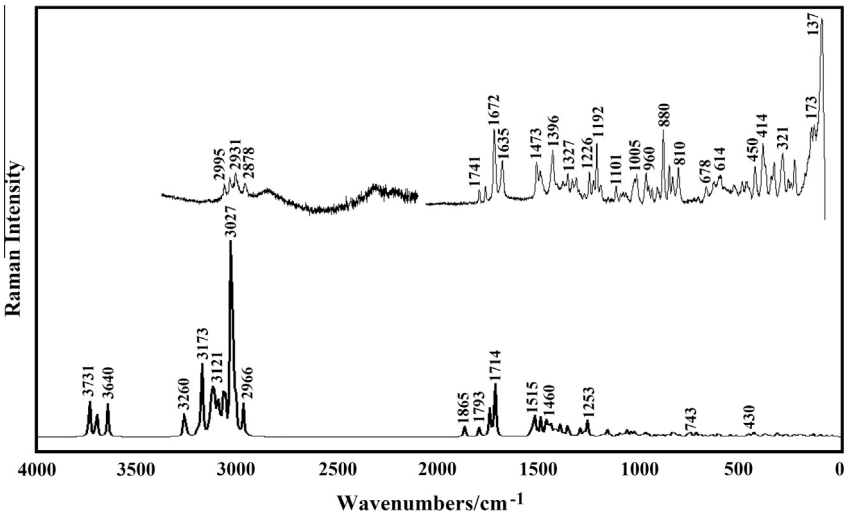

Fig. 3. Comparison between the experimental Raman spectrum of cnicin (upper) with the corresponding theoretical at B3LYP/6-31G* level of theory (bottom).

Table 2
Observed and calculated wavenumbers (cm^{-1}) and assignment for cinicin.

IR[a] Liquid	Raman[a]	Calculated[b]	SQM[c]	IR int.[d]	Raman act.[e]	Assignment[a]
3404 sh		3731	3577	20.9	107.9	ν(O52—H53)
3342 m		3696	3543	163.4	80.2	ν(O21—H22)
3246 sh		3640	3489	97.4	94.0	ν(O47—H48)
		3260	3125	5.6	38.3	ν_{as} CH_2 (C44)
		3257	3123	2.3	68.7	ν_{as} CH_2 (C35)
		3194	3065	6.8	26.5	ν_{as} CH_2 (C1)
		3173	3042	2.9	102.8	ν_{s} CH_2 (C44)
		3171	3040	3.7	71.4	ν_{s} CH_2 (C35)
3020 w		3168	3037	7.8	34.8	ν_{as} CH_2 (C49)
	3004 vw	3134	3004	37.5	5.1	ν_{op} CH (C25,C23)
		3130	3000	26.3	91.5	ν_{as} CH_3 (C6)
	2995 vw	3121	2992	0.2	92.1	ν_{ip} CH (C25,C23)
	2985 vw	3113	2984	22.9	117.2	ν (C5—H10)
	2980 sh	3110	2982	6.5	29.7	ν (C29—H30)
		3097	2969	7.2	56.3	$\nu_{as}CH_2$ (C11)
	2955 vw	3088	2959	10.1	104.9	$\nu_{as}CH_3$ (C6)
	2942 sh	3068	2941	15.0	49.2	$\nu_{as}CH_2$ (C14)
	2936 sh	3061	2934	31.8	83.1	$\nu_{s}CH_2$ (C49)
2928 w	2931 vw	3057	2931	44.9	85.9	$\nu_{as}CH_2$ (C18)
	2910 sh	3027	2902	13.6	402.5	$\nu_{s}CH_2$ (C1)
		3026	2901	92.1	65.8	$\nu_{s}CH_2$ (C18)
	2894 vw	3021	2896	9.5	20.3	$\nu_{s}CH_3$ (C6)
		3020	2895	59.7	171.0	$\nu_{s}CH_2$ (C14)
	2886 vw	3007	2883	6.0	51.8	ν(C31—H32)
2861 w	2878 vw	3004	2880	24.3	112.3	$\nu_{s}CH_2$ (C11)
	2839 vw	2966	2843	63.6	77.8	ν(C42—H43)
1760 s	1741 vw	1865	1797	379.1	21.3	ν (C27—O28)
1700 s	1732 sh	1793	1726	253.8	18.1	ν (C39—O40)
	1672 s	1743	1677	11.2	30.1	ν (C34=C35)
	1672 s	1739	1675	1.3	32.5	ν (C4=C5)
1654 vw	1635 m	1714	1649	18.2	78.3	ν (C17=C23)
1625 vw	1635 m	1711	1645	8.0	22.8	ν (C41=C44)
1517 vw	1473 m	1537	1473	3.4	12.6	δ_{as} CH_3 (C6)
	1459 sh	1525	1459	1.7	8.0	δCH_2 (C14)
	1454 m	1523	1458	8.6	2.2	δCH_2 (C1)
	1454 m	1515	1456	4.4	24.2	δCH_2 (C49)
	1454 m	1513	1451	3.4	14.3	δCH_2 (C18)
1445 vw	1442 sh	1490	1447	6.7	22.9	$\delta_{as}CH_3$ (C6)
1431 vw	1437 sh	1486	1431	7.1	15.7	δCH_2 (C44)
	1424 sh	1460	1426	5.1	24.7	δCH_2 (C11)
1415 vw	1417 sh	1457	1416	15.3	15.0	wag CH_2 (C11)
		1448	1407	12.0	10.1	ν (C17—C18)
	1396 s	1440	1403	15.7	10.4	wag CH_2 (C18)
	1396 s	1439	1401	65.0	4.4	wag CH_2 (C49)
1397 w	1396 s	1433	1395	25.1	14.9	β(C5—H10), ν (C1—C4)
	1396 s	1422	1394	3.4	5.3	τwCH_2 (C35)
1390 sh	1396 s	1414	1390	10.4	8.8	$\delta_{s}CH_3$ (C6)
1377 sh	1377 w	1411	1379	33.1	7.7	ρC29—H30
		1408	1370	5.8	0.5	$wagCH_2$ (C1)
	1364 w	1395	1364	2.7	3.4	$wagCH_2$(C14)
	1364 w	1392	1363	1.8	14.9	$wagCH_2$ (C14)
	1364 w	1389	1362	4.1	3.2	δ (O21—H22), ρCH_2(C18)
1344 vw	1351 m	1386	1356	22.1	3.9	ρC31—H32
	1338 w	1371	1338	2.1	0.7	ρ'C25—H33, β (C23—H24)
	1338 w	1369	1335	106.2	5.7	ρC42—H43
	1338 w	1353	1332	3.8	15.8	ρCH_2(C49)
1325 vw	1328 m	1347	1325	65.8	5.5	ρC25—H33
	1307 m	1321	1310	1.4	3.0	ρ'C42—H43
1284 m	1296 w	1295	1291	88.8	2.7	ρCH_2(C1)
	1287 m	1294	1268	34.3	7.5	ρ'C29—H30
1260 s	1275 w	1290	1260	28.7	7.6	ρCH_2(C11)
	1262 vw	1271	1255	44.0	7.5	δ(O47—H48)
1243 sh	1250 vw	1262	1238	24.2	3.3	ν (C27—C34)
	1226 m	1253	1222	7.0	29.3	ν (C14—C17)
1214 s	1208 m	1229	1220	26.0	0.8	ρCH_2(C14)
1197 sh	1192 s	1215	1194	110.8	0.8	ρ'C31H32
	1173 w	1193	1178	14.6	1.1	ν (C39—O38)
1161 s	1160 vw	1185	1160	14.2	2.9	ν (C4—C6)
1147 sh	1155 vw	1174	1149	325.5	2.8	δO26C25C23
	1136 vw	1160	1135	113.9	3.4	δ(O52—H53), ν (C41—C42)
	1122 vw	1155	1127	16.6	9.6	ν (C27—O26), β C27=O28
1115 sh	1115 vw	1136	1117	35.2	2.8	ν (C23—C25), ρCH_3
1094 m	1101 w	1111	1092	61.8	3.2	ν (C5—C11)

(*continued on next page*)

Table 2 (*continued*)

IR[a] Liquid	Raman[a]	Calculated[b]	SQM[c]	IR int.[d]	Raman act.[e]	Assignment[a]
1082 sh	1081 vw	1098	1075	46.2	0.5	ρCH_3
	1073 sh	1093	1065	26.8	4.7	ν (C42—O47)
1051 sh	1069 vw	1082	1052	21.8	1.2	ν (C29—C31)
	1056 vw	1071	1051	35.0	5.3	ν (C18—O21)
1043 m	1047 vw	1057	1032	15.9	8.4	ν (C25—C31)
1029 s	1024 sh	1054	1026	14.9	2.6	ν (C49—O52)
1010 sh	1014 m	1039	1013	0.2	7.2	ν (C11—C14)
998 sh	1005 m	1026	992	73.6	3.5	ν (C25—O26)
	991 sh	1020	984	12.6	6.8	ν (C31—C34)[#]
		1009	979	186.9	2.2	δC29C31C34
		998	971	45.5	1.4	ν (C29—O38)
	960 m	984	959	9.7	1.9	γ(C5—H10)
	960 m	972	956	8.1	2.9	wag CH_2(C44)
954 s		969	954	8.8	3.4	wagCH_2(C35)
947 sh	949 w	966	947	48.4	1.4	ρCH_2(C44)
	932 w	963	945	14.5	1.4	γ(C23—H24)
928 w		952	921	7.8	5.9	τwCH_2(C35)
897 w	909 w	923	902	6.1	3.1	δC29C31C34
875 vw	895 sh	902	874	3.7	3.1	ν (C29—C1)
	880 s	892	867	19.1	1.9	τw CH_2(C18)
851 vw	852 m	879	845	4.0	2.6	τwCH_2(C49)
	836 m	855	834	4.7	5.3	γ(C27=O28)
	836 m	831	828	8.3	4.3	τwCH_2(C1) [#]
812 w	810 m	826	811	7.2	6.8	βR_4 (A10)[#]
752 vs	796 vw	810	789	4.3	3.0	βR_1 (A10)
752 vs	753 vw	797	786	5.2	3.0	γ(COO)
752 vs	748 vw	755	781	5.8	5.3	γ(COO), ν (C39—C41)
	735 vw	745	732	10.3	6.0	τwCH_2(C14)[#]
716 sh	717 vw	743	706	5.1	2.1	τwCH_2(C11)
	702 vw	715	697	7.1	5.9	ρCOO
		693	685	3.3	3.6	δC29C31C34
679 sh	678 w	684	679	4.6	1.8	βR_2 (A5)
668 s	662 vw	668	660	5.4	1.7	τwCH_2(C44)
654 sh	643 m	643	641	3.8	1.3	ρCH_2(C35) [#]
	632 w	633	626	19.7	2.9	βR_1 (A5)
	621 m	608	621	29.0	1.2	βR_7 (A10)
	614 m	603	592	40.3	4.2	δCOO
	600 w	601	583	104.9	1.7	δO47C42C41
	584 w	559	552	2.3	0.7	δC29O38C39[#]
	576 w	545	540	17.7	2.0	τO47H48
	565 w	539	527	45.9	1.4	δO47C42C41, δO47C42C49
	550 w	519	515	50.5	2.7	δO47C42C41
	510 m	459	473	6.5	3.5	τO21H22
	491 m	453	447	1.7	2.4	δO26C25C23
	488 m	442	446	0.8	1.2	γ(C17—C18)
	450 m	430	432	4.3	5.1	δ O26C25C23
		424	417	3.6	2.8	δO38C29C1, βC17—C18
	414 s	413	413	0.6	2.7	τR_2 (A10)
	385 vw	375	405	2.1	4.3	βC4—C6, γ(C4—C6)
	374 m	367	370	90.8	2.6	βR_5 (A10)
	361 m	358	357	15.5	1.2	τR_1 (A5)
	344 vw	346	342	6.1	1.8	γ(C34=C35)
	321 s	316	329	1.0	3.0	τO52H53
		310	312	0.8	2.1	τR_1 (A10)
	301w	307	307	6.2	2.1	ρC1=C44, ρC34=C35
	294 m	292	294	5.4	1.1	δC42C49O52[#]
	282 m	271	288	5.7	3.5	δO26C25C23
	265 m	268	267	1.8	1.6	βR_6 (A10)
	237 vw	236	255	1.7	0.3	τR_3 (A10)
	231 w	230	238	0.9	2.3	δC29O38C39[#]
	223 w	224	221	0.8	1.1	βR_3 (A10)
	211 sh	207	211	0.6	2.3	τR_4 (A10)
	200 m	204	205	2.9	1.1	τR_5 (A10)
	186 s	192	189	0.2	1.9	γ(C41=C44) [#]
	186 s	180	186	0.6	1.2	βR_2 (A10)
	173 s	173	169	3.8	1.2	δC42C41C39
		150	164	1.3	0.6	τwCH_3
		145	138	0.2	1.5	τR_2 (A5) [#]
	137 vs	133	125	1.2	1.1	τR_5 (A10)
		129	121	0.5	2.9	τR_6 (A10)
		118	113	0.7	0.3	τ(C49—C42)
		99	107	2.6	2.0	τ(C18—C17)
		95	91	1.6	1.8	τR_1 (A5)
		70	83	3.1	1.2	δC29C31C34
		65	65	1.1	0.5	Butt

Table 2 (*continued*)

IR[a] Liquid	Raman[a]	Calculated[b]	SQM[c]	IR int.[d]	Raman act.[e]	Assignment[a]
		49	57	2.4	0.4	τR_1(A10)
		38	40	0.5	1.4	τ(COO)
		27	34	2.3	0.4	τ(C29—O38)
		14	23	0.2	0.9	τ (C42—C41)

Abbreviations: ν, stretching; β, deformation in the plane; γ, deformation out of plane; wag, wagging; τ, torsion; β_R, deformation ring τ_R, torsion ring; ρ, rocking; twis, twisting; α, angular deformation; δ, deformation; Butt, butterfly; a, antisymmetric; s, symmetric; A5, Five members Ring; A10, Ten members Ring; ip, in-phase; op, out-of-phase.

[a] This work.
[b] DFT B3LYP/6-31G*.
[c] From scaled quantum mechanics force field.
[d] Units are km mol^{-1}.
[e] Raman activities in Å^4 (amu)$^{-1}$.
[#] Assigned by *GaussView* program [40].

groups [1–5,7,9,11,13,14,16,18,19,23], the form and broadness of those IR bands most likely indicate the existence of intra-molecular O—H···O bonds, which is in agreement with the results obtained by AIM analysis. The corresponding deformation modes were predicted at 1362, 1255 and 1135 cm^{-1}, which were assigned to the Raman bands at 1364, 1262 and 1136 cm^{-1}, respectively. The torsion modes were assigned in accordance with the calculations to the Raman bands at 576, 510 and 321 cm^{-1}.

4.5.1.2. CH modes. The C23—H24 stretching is predicted to be coupled to the C25—H33 stretching, and the calculated SQM for both the out-of-phase and in-phase modes is predicted to be 3004 and 2992 cm^{-1}, respectively, as observed in Table 2. The Raman bands located at 3004 and 2995 cm^{-1} are thus assigned to those vibration modes. The remaining CH vibration modes are assigned as indicated in Table 2.

4.5.1.3. CH_3 modes. The nine expected vibration modes corresponding to this group were easily assigned, taking into account the higher PED contribution. Thus, the Raman bands at 3004 and 2955 cm^{-1} are assigned to the antisymmetric stretching modes, while the corresponding symmetric stretching mode is assigned to the Raman band at 2894 cm^{-1}. A antisymmetric CH_3 deformation mode is predicted to overlap with a CH_2 deformation, as observed in Table 2. Therefore, the three deformation modes are associated with the IR bands at 1517, 1445 and 1390 cm^{-1}. The symmetric deformation mode is assigned to the strong Raman band at 1396 cm^{-1}. The rocking and twisting modes are clearly predicted in the expected regions [1,3,11,13,14,16,18,19,23], and they were assigned accordingly, as observed in Table 2.

4.5.1.4. CH_2 modes. Cnicin has five CH_2 groups and two C=CH_2 groups; ten stretching modes are expected for the first group and four for the second one. The stretching modes of both groups can be easily assigned to the bands located in the 3260–3020 cm^{-1} region, as observed in Table 2. The bending or deformation modes are predicted to be between 1459 and 1426 cm^{-1}, and they were assigned to the bands between 1460 and 1424 cm^{-1}. Five wagging modes were assigned to the bands between 1415 and 1364 cm^{-1}, and the two remaining modes were assigned to the Raman and IR bands at 960 and 954 cm^{-1}, respectively. The five expected CH_2 rocking modes were assigned to the Raman bands between 1364 and 1208 cm^{-1} and the modes corresponding to the C=CH_2 groups at 949 and 643 cm^{-1}, as indicated in Table 2. Finally, the IR and Raman bands at 928, 851, 668, 880, 836, 735 and 717 cm^{-1} are associated with the twisting modes.

4.5.1.5. CO modes. The SQM calculations clearly predicted that the two C=O stretching modes belong to the COO group and the lactone ring of cnicin at 1797 and 1726 cm^{-1}. Therefore, both modes are easily assigned to the strong IR bands at 1760 and 1700 cm^{-1}. Both bands are predicted to have an inverted intensity relation with respect to the experimental IR spectrum, as observed in Fig. 2. The C=O in-plane and out-of-plane deformation modes corresponding to the lactone ring are assigned to the Raman bands at 1122 and 836 cm^{-1}, respectively. For the COO group, the in-plane deformations, out-of-plane deformations, and rocking and twisting modes are predicted at 592, 702, 753 and 30 cm^{-1}, respectively, as indicated in Table 2. For COO, only the twisting mode was not assigned.

4.5.1.6. Skeletal modes. Cnicin has two C=C stretching modes belonging to the ten membered ring and two C=CH_2 stretching modes. Four bands are expected in the 1677–1645 cm^{-1} region, as predicted by SQM calculations. These four stretching modes were predicted to have higher intensities in the Raman spectrum than in the IR spectrum; hence, they were assigned to the Raman bands at 1672 and 1635 cm^{-1}. The C=CH_2 in-plane and out-of-plane deformation modes were assigned in the lower wavenumbers region, and as predicted by calculations, they were assigned to the Raman bands at 344, 301 and 186 cm^{-1}, respectively. The very strong IR band at 752 cm^{-1}, which is principally attributed to the C39—C41 stretching mode, is justified because its bond is conjugated with two double bonds (C44=C41—C39=O40), as observed in Fig. 2. The remaining skeletal modes were assigned and can be observed in Table 2.

5. Force field

The force constants expressed by internal coordinates were calculated from the corresponding scaled force fields at the B3LYP/6-31G* level of theory employing the SQM methodology [39] and the Molvib program [45]. The force constant values for cnicin are shown in Table 3 and were compared with those reported for another sesquiterpenoid, dehydrofukinone [23]. The slightly higher values of the $f(\nu C{=}O)$, $f(\nu C{=}C)$, $f(\nu CH_2)sp^3$ force constants for cnicin compared to dehydrofukinone are directly related to the presence of two C=O bonds, four C=C bonds and five CH_2 groups; in dehydrofukinone, only a C=O bond, two C=C bonds and three CH_2 groups exist. On the contrary, the slightly higher value of the $f(\nu CH_3)$ force constant for dehydrofukinone compared to cnicin is due to the presence of four CH_3 groups in dehydrofukinone, while there is only one CH_3 group in cnicin. In general, the calculated force constant values are in accordance with the values reported for molecules containing similar groups [1,3,5,7–11,13–16,18–23].

6. Ultraviolet–visible spectrum

Fig. 4 shows the electronic spectrum of cnicin in a methanol (MeOH) solution phase compared to the calculated spectrum at

Table 3
Comparison of scaled internal force constants for cnicin.

Force constant	B3LYP/6-31G*[a]	B3LYP/6-31G*[b]
f(νO—H)	6.99	
f(νC═O)	12.40	11.11
f(νC—O)	5.44	
f(νC═C)	9.20	8.46
f(νCH$_2$)sp^3	4.79	4.76
f(νCH$_2$)sp^2	5.22	
f(νCH$_3$)	4.18	4.87
f(δCH$_2$)sp^3	0.76	0.73
f(δCH$_2$)sp^2	0.44	
f(δCH$_3$)	0.56	0.55

Units are mdyn Å^{-1} for stretching and stretching/stretching interaction and mdyn Å rad^{-2} for angle deformations.
[a] This work.
[b] From Ref. [23].

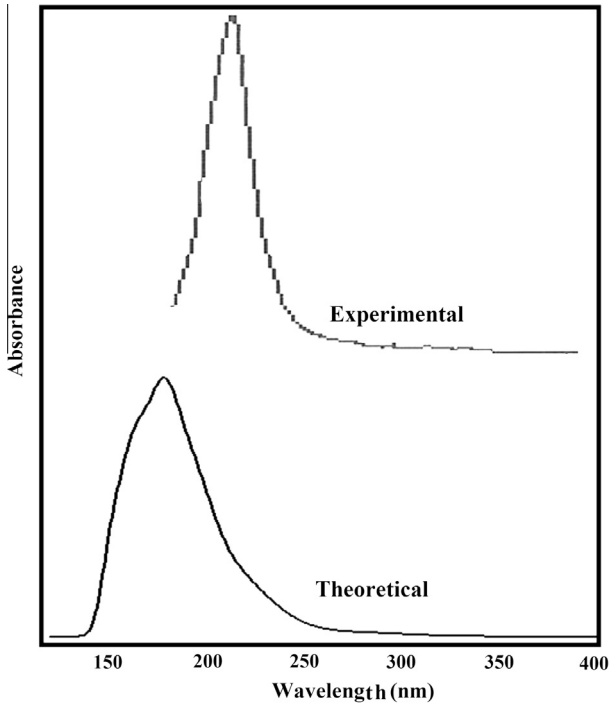

Fig. 4. Experimental in methanol solution (upper) and theoretical (bottom) ultraviolet–visible spectrum of cnicin.

the B3LYP/6-31G* level. Only intense experimental and theoretical bands are observed at 225 and 180 nm, respectively, with the latter having a predicted band energy of 6.8879 eV and an oscillator strength of f = 0.2084, which should be assigned to the chromophore present in the molecule. In other similar sesquiterpenic compounds, the intense band is observed in MeOH between 220 and 208 nm [49–51]. Cnicin most likely experiences a negative Cotton effect that can be attributed to the π → π* transition in an α,β-unsaturated γ-lactone at 218 nm in MeOH, as reported by Uchida and Kuriyama [52]. The sign of the Cotton effect is therefore determined by the chirality of the C═C—C═O chromophore; in cnicin, the calculations predict negative C35═C34—C27═O28 torsion angles, as observed in Table 1 and reported by Bovill et al. for costunolide [47].

7. Conclusions

Cnicin was isolated and characterized using infrared, Raman, NMR and UV–visible spectroscopies. The theoretical molecular structure of cnicin was determined by employing the B3LYP/6-31G* method and was determined to have two fused rings, one planar with five members and another with ten members that adopts a chair conformation. The γ-lactone ring has a half-chair conformation, which is characteristic of a *trans* lactone with negative C═C—C═O torsion angles. Therefore, cnicin experiences a negative Cotton effect, which can be attributed to the π → π* transition in an α,β-unsaturated γ-lactone, as reported in the literature. The NBO and AIM studies show that the high stability of cnicin is related to the presence of OH groups, a COO group and a lactone ring as well as three different types of hydrogen bonds. A complete assignment of the 153 normal vibration modes of the compound was performed, taking into account the SQM force field employing the B3LYP/6-31G* combination. The calculated force constant values are in accordance with the values reported for similar molecules. The combination of solution IR, Raman, NMR and UV–visible spectra and computational methods supports the experimental information about the intermolecular interactions of cnicin.

Acknowledgements

This work was supported with grants from CIUNT (Consejo de Investigaciones, Universidad Nacional de Tucumán) and CONICET (Consejo Nacional de Investigaciones Científicas y Técnicas, R. Argentina). The authors would like to thank Prof. Tom Sundius for his permission to use MOLVIB.

Appendix A. Supplementary material

Supplementary data associated with this article can be found, in the online version, at http://dx.doi.org/10.1016/j.molstruc.2014.02.057.

References

[1] E. Romano, A.B. Raschi, A. Benavente, S.A. Brandán, Spectrochim. Acta, Part A 84 (2011) 111–116.
[2] C.D. Contreras, A.E. Ledesma, H.E. Lanús, J. Zinczuck, S.A. Brandán, Vibrat. Spectr. 57 (2011) 108–115.
[3] G.R. Argañaraz, E. Romano, J. Zinczuk, S.A. Brandán, J. Chem. Chem. Eng. 5 (8) (2011) 747–758.
[4] C.D. Contreras, A.E. Ledesma, J. Zinczuk, S.A. Brandán, Spectrochim. Acta, Part A 79 (2011) 1710–1714.
[5] L.C. Bichara, H.E. Lanús, S.A. Brandán, J. Chem. Chem. Eng. 5 (2011) 936–945.
[6] S.A. Brandán, E. Eroğlu, A.E. Ledesma, O. Oltulu, O.B. Yalçınkaya, J. Mol. Struct. 993 (2011) 225–231.
[7] C.D. Contreras, M. Montejo, J.J. López González, J. Zinczuk, S.A. Brandán, J. Raman Spectrosc. 42 (1) (2011) 108–116.
[8] E. Romano, N.A.J. Soria, R. Rudyk, S.A. Brandán, J. Molec. Simul. 38 (7) (2012) 561–566.
[9] A.B. Brizuela, L.C. Bichara, E. Romano, A. Yurquina, S. Locatelli, S.A. Brandán, Carbohydr. Res. 361 (2012) 212–218.
[10] M.V. Castillo, E. Romano, A.B. Raschi, A. Yurquina, S.A. Brandán, Comput. Theoret. Chem. 995 (2012) 43–48.
[11] E. Lizarraga, E. Romano, R. Rudyk, C.A.N. Catalán, S.A. Brandán, Spectrochim. Acta, Part A 97 (2012) 202–208.
[12] A. Brizuela, E. Romano, A. Yurquina, S. Locatelli, S.A. Brandán, Spectrochim. Acta, Part A 95 (2012) 399–406.
[13] E. Romano, M.V. Castillo, J.L. Pergomet, J. Zinczuk, S.A. Brandán, J. Mol. Struct. 1018 (2012) 149–155.
[14] P. Leyton, C. Paipa, A. Berrios, A. Zárate, S. Fuentes, M.V. Castillo, S.A. Brandán, Spectrochim. Acta, Part A 88 (2012) 162–170.
[15] E. Romano, N.A.J. Soria, R. Rudyk, S.A. Brandán, J. Asia Spect. 17 (2013) 1–28.
[16] E. Romano, M.V. Castillo, J.L. Pergomet, J. Zinczuk, S.A. Brandán, Open J. Synthesis, Theory Appl. 2 (2013) 8–22.
[17] A.B. Brizuela, A.B. Raschi, M.V. Castillo, P. Leyton, E. Romano, S.A. Brandán, Comput. Theoret. Chem. 1008 (2013) 52–60.
[18] O.E. Piro, G.A. Echeverría, E. Lizarraga, E. Romano, C.A.N. Catalán, S.A. Brandán, Spectrochim. Acta, Part A 101 (2013) 196–203.
[19] P. Leyton, C. Paipa, A. Berrios, A. Zárate, S. Fuentes, M.V. Castillo, S.A. Brandán, J. Mol. Struct. 1031 (2013) 110–118.
[20] E. Romano, A.B. Brizuela, K. Guzzetti, S.A. Brandán, J. Molec. Struct. 1037 (2013) 393–401.
[21] E. Romano, F. Ladetto, S. Antonia Brandán, Comput. Theoret. Chem. 1011 (2013) 57–64.

[22] L.C. Bichara, S.A. Brandán, J. Molec. Liq. 181 (2013) 34–43.
[23] E. Lizarraga, E. Romano, A.B. Raschi, P. Leyton, C. Paipa, C.A.N. Catalán, S.A. Brandán, J. Molec. Struct. 1048 (2013) 331–338.
[24] G. Nowak, M. Holub, M. Budesinsky, Acta Soc. Bot. Pol. 58 (1989) 95–102.
[25] L.P. Christensen, J. Lam, Phytochemistry 29 (1990) 2753–2785.
[26] L.P. Christensen, J. Lam, Phytochemistry 30 (1991) 3289–3292.
[27] I. Landau, H. Mueller-Scharer, P.I. Ward, J. Chem. Econ. 20 (1994) 929–942.
[28] Anke Steinbach, Axel J. Scheidig, Christian D. Klein, J. Med. Chem. 51 (16) (2008) 5143–5147.
[29] A.M. Fortuna, E.C. Riscala, C.A.N. Catalán, T.E. Gedris, w. Herz, Biochem. Syst. Econ. 29 (2001) 967–971.
[30] A.M. Fortuna, E.C. Riscala, C.A.N. Catalán, T.E. Gedris, w. Herz, Biochem. Syst. Econ. 30 (2002) 805–808.
[31] M.E. Sesto Cabral, A.M. Fortuna, E.C. Riscala, C.A.N. Catalán, E.E. Sigtad, Allelopathy J. 21 (2008) 175–183.
[32] K. Jöhrer, Obkircher, D. Neureiter, J. Parteli, C. Zelle-Rieser, E. Maizner, J. Kern, M. Hermann, F. Hamacher, O. Merkel, N. Wacht, C. Zidorn, M. Scheideler, R. Greil, J. Mol. Med. 90 (6) (2012) 681–693.
[33] R.K. Anchoori, M.S. Quirine Kortenhorst, M. Hidalgo, T. Sarkar, G. Hallur, R. Bai, P.J. Van Diest, E. Hamel, S.R. Khan, J. Med. Chem. 51 (19) (2008) 5953–5957.
[34] A.E. Reed, L.A. Curtis, F. Weinhold, Chem. Rev. 88 (6) (1988) 899–926.
[35] E.D. Glendening, J.K. Badenhoop, A.D. Reed, J.E. Carpenter, F. Weinhold, NBO 3.1; Theoretical Chemistry Institute, University of Wisconsin, Madison, WI, 1996.
[36] R.F.W. Bader, Atoms in Molecules, A Quantum Theory, Oxford University Press, Oxford, 1990 (ISBN: 0198558651).
[37] F. Biegler-Köning, J. Schönbohm, D. Bayles, J. Comput. Chem. 22 (2001) 545–559.
[38] R.G. Parr, R.G. Pearson, J. Am. Chem. Soc. 105 (1983) 7512–7516.
[39] (a) G. Rauhut, P. Pulay, J. Phys. Chem. 99 (1995) 3093–3100;
(b) G. Rauhut, P. Pulay, J. Phys. Chem. 99 (1995) 14572.
[40] A.B. Nielsen, A.J. Holder, Gauss View 5.0, User's Reference, GAUSSIAN Inc., Pittsburgh, PA, 2009.
[41] A.D. Becke, J. Chem. Phys. 98 (1993) 5648–5652.
[42] C. Lee, W. Yang, R.G. Parr, Phys. Rev. B 37 (1988) 785–789.
[43] M.J. Frisch, G.W. Trucks, H.B. Schlegel, G.E. Scuseria, M.A. Robb, J.R. Cheeseman, J.A. Montgomery Jr., T. Vreven, K.N. Kudin, J.C. Burant, J.M. Millam, S.S. Iyengar, J. Tomasi, V. Barone, B. Mennucci, M. Cossi, G. Scalmani, N. Rega, G.A. Petersson, H. Nakatsuji, M. Hada, M. Ehara, K. Toyota, R. Fukuda, J. Hasegawa, M. Ishida, T. Nakajima, Y. Honda, O. Kitao, H. Nakai, M. Klene, X. Li, J.E. Knox, H.P. Hratchian, J.B. Cross, C. Adamo, J. Jaramillo, R. Gomperts, R.E. Stratmann, O. Yazyev, A.J. Austin, R. Cammi, C. Pomelli, J.W. Ochterski, P.Y. Ayala, K. Morokuma, G.A. Voth, P. Salvador, J.J. Dannenberg, V.G. Zakrzewski, S. Dapprich, A.D. Daniels, M.C. Strain, O. Farkas, D.K. Malick, A.D. Rabuck, K. Raghavachari, J.B. Foresman, J.V. Ortiz, Q. Cui, A.G. Baboul, S. Clifford, J. Cioslowski, B.B. Stefanov, G. Liu, A. Liashenko, P. Piskorz, I. Komaromi, R.L. Martin, D.J. Fox, T. Keith, M.A. Al-Laham, C.Y. Peng, A. Nanayakkara, M. Challacombe, P.M.W. Gill, B. Johnson, W. Chen, M.W. Wong, C. Gonzalez, J.A. Pople, Gaussian 09, Revision A.02, Gaussian Inc., Pittsburgh, PA, 2009.
[44] B.H. Besler, K.M. Merz Jr., P.A. Kollman, J. Comp. Chem. 11 (1990) 431–439.
[45] T. Sundius, Vib. Spectrosc. 29 (2002) 89–95.
[46] R. Ditchfield, Mol. Phys. 8 (1974) 397–409.
[47] M.J. Bovill, P.J. Cox, P.D. Cradwick, M.H.P. Guy, G.A. Sim, D.N.J. White, Acta Cryst. B32 (1976) 3203–3209.
[48] S. Berger, D. Sicker, Classics in Spectroscopy, Isolation and Structure Elucidation of Natural Products, Wiley-VCH, 2009.
[49] H.-Y. Liu, X.-H. Ran, N.-B. Gong, W. Ni, X.-J. Qin, Y.-Y. Hou, Y. Lü, C.-X. Chen, Phytochemistry 88 (2013) 112–118.
[50] Z. Hassan, H. Hussain, V.U. Ahmad, S. Anjum, G. Pescitelli, T. Kurtá, K. Krohn, Tetrahedron: Asym. 18 (2007) 2905–2909.
[51] Y. Li, C.-W. Li, C.-B. Cui, X.-Z. Liu, Y.-S. Che, Nat. Prod. Bioprospect. 2 (2012) 70–75.
[52] I. Uchida, K. Kuriyama, Tetrahedron Lett. 43 (1974) 3761–3764.